

# Tuning the mechanical properties of silica microcapsules

Lijuan Zhang,<sup>a</sup> Maria D'Acunzi,<sup>a</sup> Michael Kappl,<sup>a</sup> Arnout Imhof,<sup>b</sup>  
Alfons van Blaaderen,<sup>b</sup> Hans-Jürgen Butt,<sup>a</sup> Robert Graf<sup>a</sup> and Doris Vollmer\*<sup>a</sup>

Received 13th June 2010, Accepted 16th September 2010

DOI: 10.1039/c0cp00871k

Heat treatment is a standard method to increase the hardness of silica in various applications. Here, we tested the effect of high temperature annealing on the mechanical properties of silica microcapsules by force spectroscopy under point loads applied to the particle shell. The Young's modulus of the shells moderately increases after annealing at temperatures above 500 °C. Temperatures over 850 °C result in a much stronger increase and the Young's modulus is close to that of fused silica after annealing at 1100 °C. NMR analysis revealed that in untreated microcapsules synthesized by seeded growth using the Stöber method only 55% of the silicon atoms form siloxane bonds with four neighbors, whereas the remaining ones only form three or less siloxane bonds each and, thus, a large number of ethoxy and silanol groups still exist. During annealing at 500 °C, these are successively transformed into siloxane bonds through condensation reactions. This process correlates with only a moderate increase in Young's modulus. The strong increase at temperatures above 850 °C was associated with a densification which was associated by a decrease in capsule size and shell thickness while the shells remained homogenous and of spherical shape. The main strengthening of the shells is thus mainly due to compaction by sintering at length scales significantly larger than that of local siloxane bonds.

## 1. Introduction

Capsules of sub-micrometre size (microcapsules) offer advantages in a wide spectrum of applications such as drug delivery,<sup>1,2</sup> bioencapsulation,<sup>3,4</sup> medical diagnostics,<sup>5</sup> catalysis,<sup>6</sup> plasmonics,<sup>7</sup> *etc.* In particular, their low density, low heat conductivity, and low refractive index that can be matched by many organic liquids are desirable in composite electronics and structural materials.<sup>8,9</sup>

Various methods have been developed for preparing nano- or microcapsules. Most common is bead templating, where polymer latexes, inorganic particles, or bubbles serve as templates.<sup>10–14</sup> In bead templating the shell thickness can be tuned to a large extent. Subsequently, the cores are removed by dissolution in a suitable solvent or by heat treatment.

For most applications, wall permeability, adhesion, friction, and mechanical stability are crucial as they have a large influence *e.g.* on transport properties. Mechanical behavior of microcapsules has been studied by osmotically induced buckling,<sup>15</sup> swelling of polyelectrolyte-filled capsules,<sup>16</sup> and deformation under a force load applied by atomic force microscopy (AFM). Of these approaches, AFM is especially suitable because force loads are applied with high precision and even nanometre deformations can be detected.<sup>17–30</sup>

The mechanical properties of microcapsules depend on the encapsulated fluid and shell thickness, and additionally on pH (surface charge) and salt concentration (ionic strength) if capsules are kept in an aqueous medium.<sup>19,20</sup> For example, polyelectrolyte microcapsules are more rigid when filled with

a polyelectrolyte solution than when filled with water.<sup>20</sup> However, although there are various possibilities of varying the stability of microcapsules, it is still a challenge to precisely tune their mechanical strength.

In this work, we synthesized hollow silica particles with polystyrene cores as templates. To test the effect of heat treatment on the mechanical properties of the resulting silica shells, we measured the Young's modulus of capsules treated at a range of different temperatures by AFM under a point load. The effect of chemical and morphological changes in the shell evoked by a specific treatment was analyzed quantitatively by AFM and the underlying molecular and structural changes evaluated by nuclear magnetic resonance (NMR). These results can provide a basis for fine-tuning the preparation process in order to achieve desired changes in mechanical stability.

## 2. Experimental section

### 2.1 Preparation of hollow silica spheres

Polystyrene (PS) beads were prepared by dispersion or soap-free emulsion polymerization (diameter of  $1.70 \pm 0.04 \mu\text{m}$  and  $0.79 \pm 0.07 \mu\text{m}$ , respectively) and coated with silica using the Stöber method<sup>31</sup> as reported previously.<sup>30</sup> Core-shell PS-silica particles with an external diameter of  $\sim 860 \text{ nm}$  and a shell thickness of  $\sim 37 \text{ nm}$  were heated to 500 °C for 3.5 h to remove the PS core. In order to compare the mechanical properties of silica microcapsules annealed at different temperatures, core-shell PS-silica particles with an external diameter of  $1.81 \pm 0.04 \mu\text{m}$  and a shell thickness of  $52 \pm 3 \text{ nm}$  were used. Their PS cores were removed by dissolving in toluene for about one week and washed in toluene at least 3 times. Then these silica microcapsules were stored in ethanol and annealed for 3.5 h at temperatures ranging from 240 °C to 1150 °C. The annealed shells were redispersed in ethanol.

<sup>a</sup> Max Planck Institute for Polymer Research, Ackermannweg 10, 55128 Mainz, Germany. E-mail: vollmerd@mpip-mainz.mpg.de; Tel: +49 6131 379 113

<sup>b</sup> Soft Condensed Matter, Debye Institute for Nanomaterials Science, Utrecht University, Princetonplein 5, 3584 CC Utrecht, The Netherlands

## 2.2 Electron microscopy

The size of the microcapsules before and after annealing was measured by low voltage scanning electron microscopy (LEO 1530 Gemini SEM, Oberkochen, Germany). Silica capsules were also imaged by transmission electron microscopy (TEM, Tecnai F20, FEI; 200 kV) to measure capsule size and shell thickness. The annealed shells were redispersed in ethanol. A few were deposited on a carbon covered copper mesh and placed in the vacuum chamber of the high resolution TEM. For each annealing temperature about 5–15 capsules were imaged. We measured the shell thickness making use of the brightness contrast of the shell compared to the interior of the capsule. This was easiest in broken shells. The thickness of each shell was measured in five places. The values given in the text are the arithmetic mean of these five values. Because the brightness edge gave rise to an uncertainty of a few nm, independent measurements were performed by three persons.

## 2.3 Solid state NMR

All solid state NMR measurements of this study were performed on a Bruker Avance II console operating at a  $^1\text{H}$  Larmor frequency of 300.23 MHz using a commercial 7 mm double resonance magic angle spinning (MAS) probe spinning at a frequency of 5 kHz. 50 kHz radio frequency (RF) nutation frequency was adjusted on both RF channels,  $^1\text{H}$  and  $^{29}\text{Si}$ , and 50 kHz hetero-nuclear dipolar decoupling was applied during acquisition using the SPINAL64 scheme. Direct excitation spectra were recorded with a tip angle of  $\sim 25^\circ$  corresponding to a pulse length of 1.4  $\mu\text{s}$  and a relaxation delay of 20 s, if not stated otherwise. All cross-polarization magic angle spinning (CP-MAS) spectra were recorded with a CP contact time of 5 ms at 5 kHz MAS spinning frequency and a repetition time of 3 s.  $^{29}\text{Si}$  chemical shifts are referenced to tetrakis(trimethylsilyl)silane.<sup>32</sup> In order to ensure sufficient protons close to the silica surface for the polarization transfer, silica surfaces were coated with polyvinylpyrrolidone (PVP, Fluka, K90,  $M_w \approx 360\,000\text{ g mol}^{-1}$ ) after high temperature annealing. Therefore the dried particles were dispersed in a mixture of ethanol and PVP (0.16 g PVP dissolved in 10 ml ethanol), the dispersion was stirred over night, cleaned and dried. The colloids investigated at room temperature and after annealing at 240  $^\circ\text{C}$  still contained a PS core, whereas the core is burned while heating the samples above 300  $^\circ\text{C}$ .

In  $^{29}\text{Si}$  MAS NMR spectra different chemical sites  $Q^n$  in the silica network can easily be distinguished, with  $n$  denoting the number of silicon atoms attached to the four oxygen atoms at the corners of a  $\text{SiO}_4$  tetrahedron.  $Q^2$  sites, corresponding to a  $\text{SiO}_4$  unit in a chain, are observed in the range from  $-85$  to  $-90$  ppm, whereas  $Q^3$  sites,  $\text{SiO}_4$  branching points in a chain, are assigned to chemical shifts around  $-100$  ppm.<sup>33,34</sup> Completely condensed  $Q^4$  sites with four attached Si sites show the lowest chemical shift values and are observed at  $-110$  ppm. The quantitative distribution of the  $Q^n$  sites in a silica network can be determined by direct excitation of the fully relaxed  $^{29}\text{Si}$  spins under MAS conditions. In many cases, however, it is difficult and very time-consuming to record these spectra, because the  $T_1$  relaxation times of silica networks are often in the range of several minutes and may differ depending on the  $Q$  site.

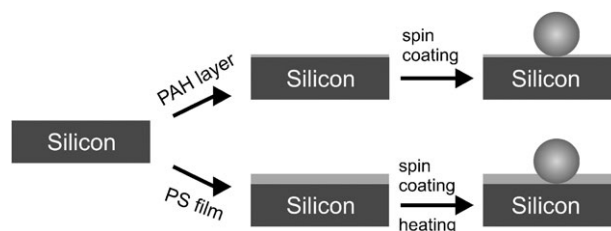
## 2.4 Preparation of samples for AFM measurements

Substrates were rinsed with milli-Q water (resistivity of 18.2  $\text{M}\Omega\text{ cm}$ ), sonicated for 10 min in ethanol, and cleaned in an Argon plasma (Plasma Cleaner, Harrick, PDC 002) at 25  $^\circ\text{C}$  with an RF power of 200 W for 5 min to remove the remaining organic substances. In order to fix the capsules on the substrate and prevent them from rolling silica capsules were partially embedded in a thin PS film (Scheme 1, bottom). The film ( $5.0\text{ mg mL}^{-1}$ ,  $M_w \approx 130\,000\text{ g mol}^{-1}$  dissolved in toluene) was obtained by spin coating (Delta 80 BM, Süs MicroTec Laboratory Equipment GMBH, Germany, 1000 rpm for 60 s) and its thickness determined with a surface profiler (KLA Tencor, LOT-Oriel GmbH & Co. KG, Germany).<sup>30</sup> The thickness ranged between 55 and 75 nm depending on position. Silica microcapsules dispersed in ethanol were coated (2000 rpm for 60 s) on the glassy PS film by spinning. The substrates were placed in an oven and kept at 150  $^\circ\text{C}$  for about 1 h. Capillary forces pull the microcapsules into the molten film and, after cooling down to room temperature, lead to a strong fixation on the substrate.

In order to test whether the PS film influences the mechanical response of the capsules, we also performed experiments with capsules fixed on a silicon substrate *via* electrostatic interactions, Scheme 1, top. For this purpose, clean silicon substrates were immersed in a solution containing 60 g of poly-allylamine hydrochloride (PAH, Aldrich, average  $M_w \approx 15\,000\text{ g mol}^{-1}$ ), 61 g of milli-Q water, and 100 mg of NaCl for 10–15 min, and then washed twice in milli-Q water. 20  $\mu\text{l}$  of an ethanol suspension of capsules with a diameter of  $\sim 860$  nm and shell thickness of  $\sim 37$  nm was then deposited on wet PAH coated silicon substrates. After deposition, the substrates were rinsed with fresh water and the excess dispersion was gently removed with filter paper. The capsules adhere to these surfaces due to electrostatic interactions between negatively charged silica and positively charged PAH and due to the formation of hydrogen bonds between the amino groups of PAH and hydroxyl groups of silica. By scratching the PAH monolayer with a sharp AFM tip the thickness of the PAH layer was determined to be about 3 nm.

## 2.5 AFM imaging and force measurements

Tapping-mode AFM imaging and force measurements were performed with a Multimode Nanoscope IIIa SPM from Digital Instruments (Veeco Metrology Group, Plainview, NY) at  $25 \pm 2$   $^\circ\text{C}$  using silicon AFM probes (OMCL-AC



**Scheme 1** Sketch of the procedures for immobilizing the microcapsules on the substrates. Immobilization was achieved by coating silicon substrates either with a positively charged PAH monolayer (top) or with a PS film (bottom). A dilute dispersion of capsules was spin coated onto the adhesive layers. Adhesion to PS films was achieved by melting and subsequently cooling the film.

160TS, Olympus, Japan) with a resonance frequency of about 300 kHz and a tip radius of less than 20 nm. The spring constants of the cantilevers were determined to be  $42 \pm 12 \text{ N m}^{-1}$  by the thermal noise method as mentioned by Hutter and Bechhoefer.<sup>35,36</sup> For each experiment, a fresh silicon substrate and a sample were mounted on the same AFM specimen holder. Before starting the force measurements, the immobilized silica microcapsules were imaged in tapping mode, and a well-shaped microcapsule was chosen. By repeatedly zooming in, we carefully located the top of the target capsule. For the ensuing

force measurements, the substrate was moved up and down periodically at a constant scan rate (1.0 Hz) while the cantilever deflection was recorded. The result was a graph of the cantilever deflection signal in volts *versus* the height position of the scanner. For each of these measurements on the microcapsules, about 60 reference curves were recorded on the bare silicon substrate to obtain the deflection sensitivity, *i.e.*, the conversion factor between the measured deflection signal in volts and the actual cantilever deflection in nanometres. Recording the deflection sensitivity before and after microcapsule experiments allowed us to rule out changes in the deflection sensitivity that might have occurred during measurements. Force *versus* distance curves were calculated from the deflection *versus* piezo position curves by multiplying the cantilever deflection with the spring constant to obtain the force and subtracting the cantilever deflection from the height position to obtain the distance. Zero distance was derived from the linear contact part of force curves as described previously.<sup>30</sup> Within a series of force measurements, the maximum cantilever deflection was increased step by step, corresponding to increasingly higher force loads on the capsules. For each experimental condition, typically three microcapsules were measured.

### 3. Results and discussion

#### 3.1 Force *versus* distance curves

Force *versus* distance curves were obtained by applying a point load to the top of the capsule with an AFM tip (Fig. 1a). TEM images show that the capsules (diameter of  $1.81 \pm 0.04 \mu\text{m}$  and thickness of  $52 \pm 3 \text{ nm}$ ) are perfectly spherical and have uniform shell thickness. At large distances, the force is zero,

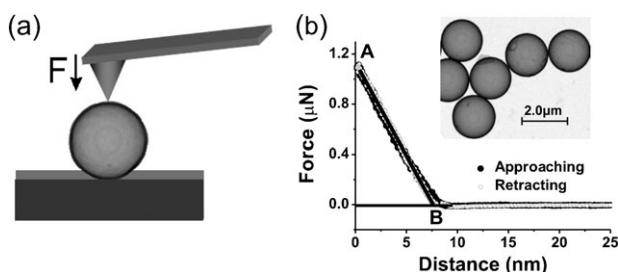


**Fig. 1** (a) Sketch of the set-up. (b) A typical force *versus* distance curve of a silica capsule. The filled and open circles denote the approaching and retracting curve, respectively. Hardly any hysteresis is visible, *i.e.*, the deformation is elastic. Inset: TEM image of silica microcapsules with a diameter of  $1.81 \pm 0.04 \mu\text{m}$  and thickness of  $52 \pm 3 \text{ nm}$ .

as the tip does not touch the capsule. As soon as the tip and capsule come into contact, the capsule starts to deform. After passing a transition region about 1 nm in width, the force increases linearly upon further approach. To obtain a force–deformation curve, we determined the deformation at maximum applied force  $F_{\text{max}}$  for each force–distance curve. This deformation is given by the intersection of the linear extrapolation of the force *versus* distance curve with the force axis (A in Fig. 1b). The corresponding maximal deformation is given by the intersection of the linear fit with the extrapolation of the zero deformation line (B in Fig. 1b). In approaching and retracting curves, no hysteresis was observed, and thus the deformation is elastic. From each such force–distance curve, one can obtain a single data point (B, A) for the corresponding force *versus* deformation dependence. Taking force curves at different defined maximum forces yields the force-*versus*-deformation curve (force curve) in Fig. 2a.

To explore the influence of the immobilization method on the force curves, we measured the deformation of 860 nm sized silica capsules either embedded in a PS film or fixed by a PAH monolayer. We chose the smaller capsules because before taking a force distance curve we had to image the surface of the particle to localize its apex. The adhesion of the  $1.81 \mu\text{m}$  sized capsules to the PAH coated substrate was too low to prevent moving of the particles while scanning the capsule. Because the elastic modulus of the shells was determined to be largely independent of sphere size within the studied size range<sup>30</sup>, we chose the type of capsules most suitable for the AFM measurements. Within experimental accuracy the fixing method did not alter the force curves (Fig. 2a). At first glance a difference might be expected because silica capsules fixed by PS sink into the film during melting of PS at  $150 \text{ }^\circ\text{C}$ .<sup>30</sup> The capsule–PS contact area  $S_{\text{PS}}$  can be estimated to be  $S_{\text{PS}} = 2\pi l_{\text{PS}}R \approx 2 \times 10^5 \text{ nm}^2$ ,<sup>37</sup> where  $R$  stands for the radius of the capsule and  $l_{\text{PS}}$  for the thickness of the PS film,  $l_{\text{PS}} = 65 \pm 10 \text{ nm}$ . PAH, in contrast, forms a 3 nm thick monolayer on silicon, *i.e.* the capsules rest on PAH coated silicon wafers. The capsule–PAH contact area  $S_{\text{PAH}} \approx 8 \times 10^3 \text{ nm}^2$  is more than an order of magnitude smaller than  $S_{\text{PS}}$ . However, according to elasticity theory the deformed area  $A$  is proportional to the radius  $R$  times the shell thickness  $h$ ,<sup>38</sup> *i.e.*  $A \propto \pi R h \approx 5 \times 10^4 \text{ nm}^2$ , which is in the same order of magnitude as the capsule–PS contact area. Because the PS-film is so thin, the capsule–PS contact can still be regarded as a point contact. Therefore both, the top as well as the bottom of the capsule are deformed.<sup>39</sup>

The independence of the preparation method is in line with our previous investigations, where we have shown that after heating the PS film above its glass transition temperature only a few nm of PS-film (2–5 nm) remain between the capsule and the substrate.<sup>30</sup> Therefore, in both cases the stiff silicon substrate is separated by a softer layer of comparable effective thickness.

Successively increasing the force loads caused the approaching and retracting curves to start to exhibit significant hysteresis until the approach curve shows a jump. The AFM image taken after this approach curve showed a hole in the shell (Fig. 2b). All measurements presented in this manuscript were taken before we saw any hint of plastic deformation.

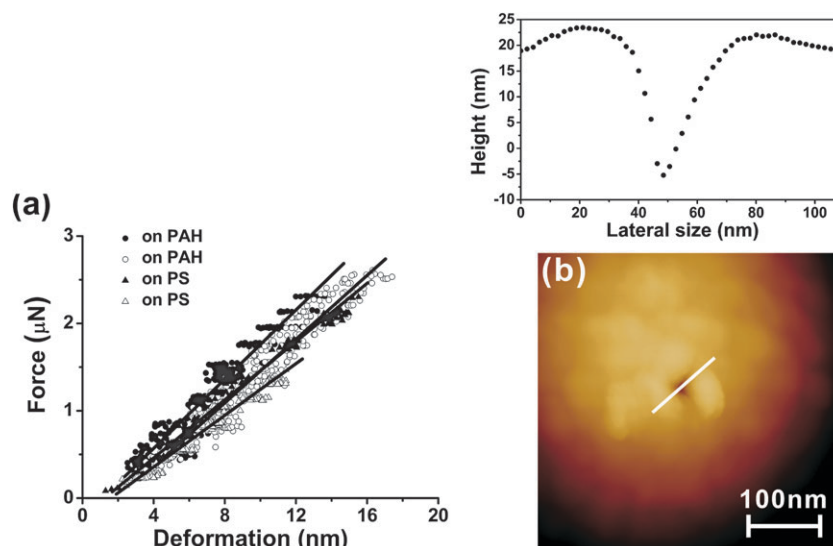


**Fig. 2** (a) Deformation of silica capsules (diameter:  $\sim 860$  nm, shell thickness:  $\sim 37$  nm) fixed on a PAH monolayer (open and filled circles) or PS film (open and filled triangles) as a function of loaded force. Open and closed symbols represent four independent measurements. The straight lines show the results of linear fits of the data. (b) Tapping mode AFM image taken after piercing into the shell together with a section analysis of the deformed area. Its direction is indicated by the white line.

### 3.2 Force-versus-deformation curves at different annealing temperatures

To investigate whether the capsule stiffness and Young's modulus depend on temperature we took force curves on  $1.81 \pm 0.04 \mu\text{m}$  sized silica capsules annealed at different temperatures (Fig. 3a). The PS cores were always removed beforehand by dissolving the particles in toluene. Complete removal was verified by TEM. Irrespective of annealing temperature, the deformation increases linearly with load-force for small deformations, in agreement with experiments after annealing at  $500^\circ\text{C}$  reported previously.<sup>30</sup> More interestingly, the stiffness, *i.e.* twice the slope of the force curve, increases slowly after annealing at temperatures up to  $850^\circ\text{C}$  and more strongly after annealing at temperatures above  $1000^\circ\text{C}$  (Fig. 3b). Here, we considered that the measured deformation is a superposition of the deformation of the top and bottom hemisphere.

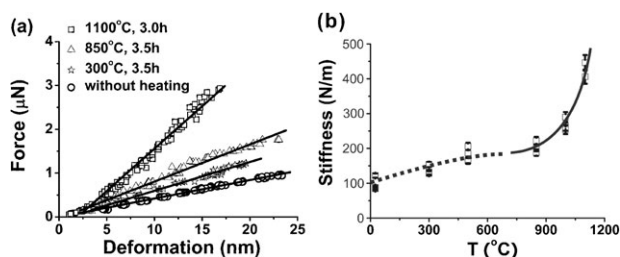


**Fig. 3** (a) Deformation of silica capsules as a function of applied load after annealing for 3.5 hours at  $300^\circ\text{C}$  ( $\star$ ),  $850^\circ\text{C}$  ( $\Delta$ ), and  $1100^\circ\text{C}$  ( $\square$ ), respectively. The sample ( $\circ$ ):  $25^\circ\text{C}$  was measured without annealing. The deformation increases linearly with applied point load. For clarity, only every third data point is shown. (b) The stiffness (force divided by deformation) increases with annealing temperature. The dotted and solid lines are guides to the eye. Capsules diameter:  $1.81 \pm 0.04 \mu\text{m}$ , shell thickness:  $52 \pm 3$  nm.

### 3.3 Dependence of the Young's modulus on annealing temperature

To calculate the Young's modulus we first measured the diameters and thicknesses of the capsules by SEM and TEM (arithmetic mean and standard deviation shown in Table 1). In SEM, diameters were measured for 40 to 180 capsules. TEM data comprise results from 5 to 15 capsules at high magnification. Diameter measurements performed by TEM tended to give slightly higher values than SEM analysis for identical samples. Since TEM values were based on a smaller number of particles, we used the SEM values for further evaluation. The shell thickness in contrast could be determined by TEM only (see darker area of the inserted image in Fig. 4). In previous measurements the shell thickness was determined from the difference between the particle diameter before and after growing the silica shell. This was not possible here, as annealing caused the diameters of silica microcapsules and their shell thickness to decrease. After annealing at  $1100^\circ\text{C}$  the particle diameter decreased by almost 20%.

We calculated the Young's modulus  $E$  of silica microcapsules according to thin shell theory.<sup>40–42</sup> It applies as long

**Table 1** SEM and TEM data of diameters and thicknesses of silica capsules before and after annealing at different temperatures. The numbers in brackets denote the number of capsules evaluated

Temperature/ $^\circ\text{C}$	Diameter/ $\mu\text{m}$ SEM	Diameter/ $\mu\text{m}$ TEM	Thickness/nm TEM
25	$1.81 \pm 0.04$ (150)	$1.83 \pm 0.04$	$52 \pm 3$
300	$1.75 \pm 0.04$ (180)	$1.80 \pm 0.04$	$43 \pm 3$
500	$1.65 \pm 0.04$ (130)	$1.72 \pm 0.04$	$43 \pm 6$
850	$1.63 \pm 0.04$ (140)	$1.72 \pm 0.03$	$43 \pm 5$
1000	$1.62 \pm 0.05$ (40)	$1.66 \pm 0.04$	$39 \pm 4$
1100	$1.52 \pm 0.04$ (140)	$1.59 \pm 0.04$	$42 \pm 7$

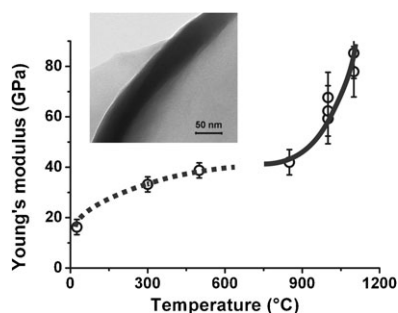


**Fig. 4** The Young's modulus increases with annealing temperature and approaches the value of fused silica after tempering at 1100 °C. The dotted and solid lines are guides to the eye. Inset: TEM image of a shell at high magnification. The dark area representing the shell shows uniform thickness.

as the reversible deformation is small, *i.e.*, if the ratio between shell thickness and capsule radius is smaller than  $\sim 1/10$ .

$$E = \frac{\sqrt{3(1-\nu^2)}FR}{4dh^2} \quad (1)$$

$d$  denotes half the measured deformation,  $h$  the shell thickness,  $R$  the radius of capsule,  $F$  the loading force, and  $\nu$  the Poisson ratio. Assuming the Poisson ratio to be  $\nu = 0.17$ ,<sup>43</sup> eqn (1) reads

$$E = 0.43 \frac{FR}{dh^2} \quad (2)$$

For annealing temperatures below 850 °C, the Young's modulus slowly increases from  $\sim 15$  to 40 GPa. Annealing at temperatures above 1000 °C causes a strong increase of the Young's modulus until it almost matches the value of fused silica, 72–76 GPa.<sup>43</sup> Surprisingly, our values slightly exceed those of fused silica.

Adhesion or embedding of the particle to the substrate could make the contact on this side larger than pointlike. This would cause a slightly lower deformation there than at the top, and thus leads to a small overestimation of  $E$ . We also cannot exclude that the applied load compresses the PS film between the capsule and the silica substrate, although its thickness has been determined to be below 5 nm.<sup>30</sup> Both effects are expected to be marginal but easily may cause an overestimation of the Young's modulus by 10%.

In contrast to the annealing temperature, the annealing time hardly had any influence on the Young's modulus. For annealing time spans of more than 1 h, increasing the annealing

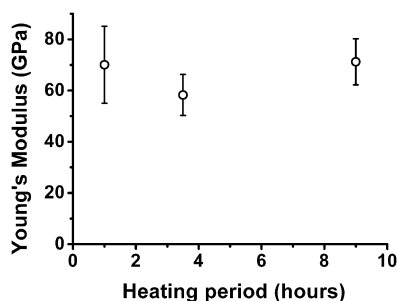


**Fig. 5** The Young's modulus as a function of heating period at 1000 °C.

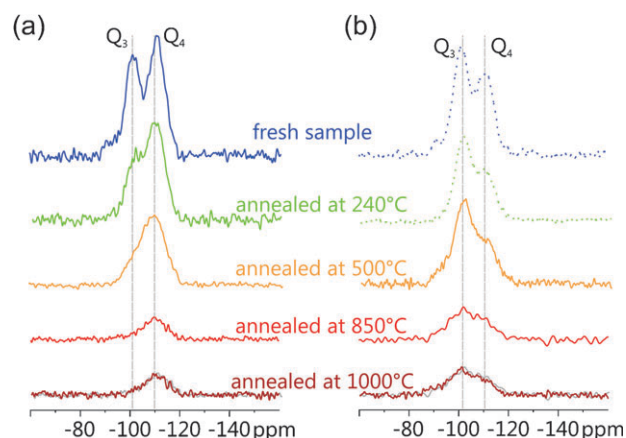


**Fig. 6** <sup>29</sup>Si magic-angle spinning nuclear magnetic resonance spectra recorded at 5 kHz MAS spinning frequency and ambient temperature. (a) Direct excitation <sup>29</sup>Si MAS NMR spectra obtained with 15 s relaxation delay between subsequent transients for the three lower temperatures and 90 s for the two highest temperatures and a low tip angle. (b) <sup>29</sup>Si cross-polarization magic-angle spinning NMR spectra recorded with 3 ms CP contact time and polyvinylpyrrolidone coating of the silica capsules after annealing.

time did not change the value of  $E$  significantly (Fig. 5). The experimental errors can be attributed to variations in shell thickness or diameter which were assumed to be identical for all capsules of the same batch.

### 3.4 Nuclear magnetic resonance

In order to relate changes in the mechanical properties to changes in chemical and physical structure during the annealing process, <sup>29</sup>Si solid state NMR measurements were performed at different stages of the annealing procedure.

<sup>29</sup>Si MAS spectra obtained from direct excitation applying <sup>1</sup>H hetero-nuclear dipolar decoupling and relaxation delays of 20 s and 90 s (samples annealed at  $T > 800$  °C) are shown in Fig. 6a. The spectrum of the freshly prepared sample shows two broad signals at  $-101$  ppm and  $-110$  ppm of similar intensity, which can be assigned to Q<sup>3</sup> and Q<sup>4</sup> sites, respectively. The relative amount of 45% Q<sup>3</sup> and 55% Q<sup>4</sup> sites was estimated by deconvolution of the two signals. A low amount of Q<sup>2</sup> site could also be present in the sample, as indicated by the weak shoulder towards lower ppm values. The substantial line width of the NMR signals is indicative of the amorphous nature of silica. Upon annealing, the amount of Q<sup>3</sup> sites is strongly reduced and after annealing at 500 °C only a minor contribution of Q<sup>3</sup> sites to the spectrum is observed, resulting in an asymmetric line shape of the Q<sup>4</sup> site signal. The observed reduction of Q<sup>3</sup> sites proves that the formation of a denser silica network containing more Q<sup>4</sup> sites starts already at relatively low temperatures.

The sample annealed at 850 °C showed a marked increase in  $T_1$  relaxation time, compared to samples annealed at lower temperatures, so that the relaxation delay had to be increased to 90 s in order to obtain a spectrum. A weak reduction of Q<sup>3</sup> sites leads to a more symmetric line shape of the Q<sup>4</sup> site signal compared to that of the sample annealed at 500 °C. The sample annealed at 1000 °C did not exhibit any changes in

the  $^{29}\text{Si}$  MAS NMR spectrum within experimental accuracy. In order to allow for easier comparison, the  $^{29}\text{Si}$  MAS NMR and  $^{29}\text{Si}$  CP-MAS NMR results of the sample annealed at  $850\text{ }^\circ\text{C}$  have been overlaid in grey colour to the NMR results of the sample annealed at  $1000\text{ }^\circ\text{C}$ . Thus, no structural changes in the silica network upon annealing at temperatures above  $850\text{ }^\circ\text{C}$  are observed.

A second solid state NMR approach *via*  $^1\text{H}$ - $^{29}\text{Si}$  CP-MAS after coating the annealed silica spheres with PVP is given in Fig. 6b. In contrast to the direct excitation method it is difficult to quantify CP-MAS measurements. The CP-MAS method relies on polarization transfer from protons located at the surface of the particle to the silica sites in the material and the transfer efficiency strongly depends on the distance between the two spins involved. Therefore the signals of  $\text{Q}^3$  sites, which in a perfect silica network are located at the surface only, are strongly over-represented. However, comparing  $^1\text{H}$ - $^{29}\text{Si}$  CP-MAS spectra recorded under the same conditions can provide additional information on possible changes in the network structure at the surface of the silica particles. The  $^1\text{H}$ - $^{29}\text{Si}$  CP-MAS spectra shown in Fig. 6b are recorded with a CP contact time of 5 ms and a repetition time of 3 s between subsequent scans, taking advantage of the short  $T_1$  relaxation time of the protons in the surface coating. For the samples without annealing or annealing at temperatures below  $300\text{ }^\circ\text{C}$ , the CP-MAS spectra are taken without PVP coating using the PS precursor particle as proton source. They are therefore displayed with dotted lines and should not be compared with the results from high temperature annealing with PVP coated particles. These two CP-MAS spectra indicate a minor reduction of  $\text{Q}^4$  sites upon low temperature annealing, unlike the results from direct excitation. This difference, however, results from a PS dewetting of the silica particles upon annealing. The fact that CP-MAS experiment monitors predominantly the particle surface, where the  $\text{Q}^3$  sites are more abundant than in the bulk, is clearly reflected in the experimental results given in Fig. 6b.  $\text{Q}^3$  sites are observed in the CP-MAS measurements, even for the samples annealed at highest temperatures, where the single pulse excitation NMR spectra suggest a very dense silica network built from  $\text{Q}^4$  sites only. Moreover, the  $^{29}\text{Si}$  CP-MAS measurements confirm the conclusion from the direct excitation results that the curing of the silica network is almost completed at an annealing temperature of  $T \approx 800\text{ }^\circ\text{C}$  and that annealing at higher temperatures does not change the ratio of  $\text{Q}^3$  and  $\text{Q}^4$  sites in the silica network. Thus the substantial increase in stiffness obtained for samples annealed at  $T = 1000\text{--}1100\text{ }^\circ\text{C}$  cannot be attributed to a significant condensation of the capsules' silica network. Moreover, it should be pointed out that the  $^{29}\text{Si}$  MAS NMR measurements do not provide any evidence for an onset of crystallization in the silica network, which would lead to much narrower NMR signals.

### 3.5 Topography of capsule's surface

Therefore we investigated the surface topography of single capsules before and after annealing by AFM. The surface of native capsules appears rough and is composed of small silica particles chemically bonded together (Fig. 7a). Annealing the

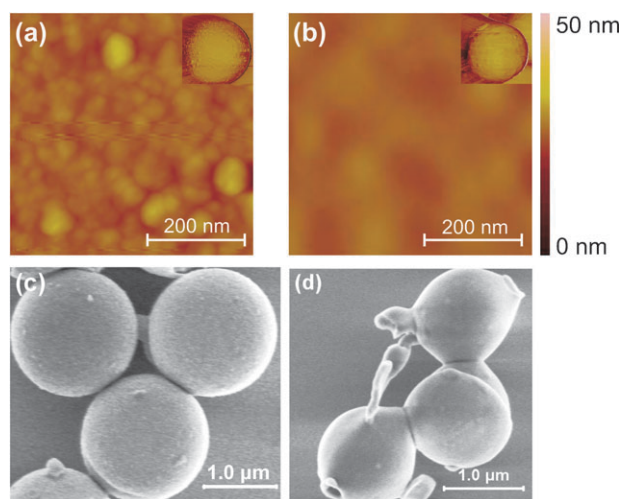


**Fig. 7** AFM height images of the surface of silica microcapsules before (a) and after (b) annealing at  $1100\text{ }^\circ\text{C}$  for 3 hours. AFM phase images of the whole capsules are given in the insets. SEM images of silica microcapsules annealed at  $1100\text{ }^\circ\text{C}$  for 3 hours (c) and  $1150\text{ }^\circ\text{C}$  for 3.5 hours (d). The surfaces of silica capsules smoothen upon heating to  $1100\text{ }^\circ\text{C}$ . The silica capsules stay spherical at  $1100\text{ }^\circ\text{C}$ , but change their morphology and begin to coalesce when annealed at  $1150\text{ }^\circ\text{C}$ .

capsules at  $1100\text{ }^\circ\text{C}$  (close to their melting point of  $\sim 1150\text{ }^\circ\text{C}$ ) causes the surface to smoothen (see Fig. 7b). Even after sintering the capsules remain intact, although both their diameter and shell thickness decrease by approximately 20%. According to SEM images, the capsules retain their spherical shape without any defects (see Fig. 7c). Smoothening also manifests itself in a decrease in RMS roughness from 1.9 nm (annealing the capsules for 3.5 h at temperatures below  $850\text{ }^\circ\text{C}$ ) to 1.0 nm after annealing the capsules for 3.5 h at  $1100\text{ }^\circ\text{C}$ . The RMS was determined on an area of  $400 \times 400\text{ nm}^2$ . Even after annealing at  $1000\text{ }^\circ\text{C}$  the AFM images almost look identical (data not shown).

When heated to  $1150\text{ }^\circ\text{C}$  the capsules start melting and their shells deform (Fig. 7d). The decrease of the RMS roughness goes in line with a decrease of the pore size. After annealing the capsules are filled with air. Redispersing in ethanol enables ethanol to diffuse into the capsules, leading to sedimentation. However, after annealing at  $850\text{ }^\circ\text{C}$  and redispersing in ethanol particles were floating, *i.e.* their pore size decreased to an extent preventing ethanol to pass the shell. This finding is supported by temperature dependent porosity measurements on porous silica films, showing a strong decrease of the porosity after annealing the films at temperatures above  $850\text{ }^\circ\text{C}$ .<sup>44</sup> It is also completely in line with temperature annealing experiments performed on photonic crystals made from Stöber silica spheres where significant compaction on larger than nm length scales was also observed only at temperatures above  $950\text{ }^\circ\text{C}$ .<sup>45</sup>

## 4. Conclusions

The Young's modulus of silica microcapsules as determined by AFM force–distance spectroscopy depends on surface and internal roughness and the number of silanol groups, which

both depend on the annealing temperature. Measurements performed after annealing at temperatures between 20 °C and 1100 °C revealed that condensation and density increase upon heat treatment is a two-step process. Heating up to 850 °C strongly decreases the number of silanol groups significantly, but leaves the grainy surface structure unmodified. The change of the local chemical bond structure causes only a moderate increase of the Young's modulus with annealing temperature. At even higher temperatures, we observed a strong increase of the Young's modulus accompanied by a smoothening of the capsule's surface and increase in density. The resulting reduction of the effective capsule surface was demonstrated by AFM imaging, where a decrease in roughness was detected. The nano-sized silica particles of which the shells are composed of fuse together at temperatures > 1000 °C. Remarkably, the capsules retain their perfect spherical shape, although the diameter and shell thickness decrease by 20%. Thus, high temperature annealing provides a method to obtain silica capsules with a completely closed shell with a thickness as thin as a few tens of nm and stiffness comparable to that of fused silica, offering new perspectives for a broad range of applications. Furthermore, characterizing the dependence of the Young's modulus on temperature and on changes in bond structure and surface morphology offers the possibility to use this dependence for tuning the mechanical properties of silica capsules.

## Acknowledgements

We are grateful to G. Schäfer for helping with the synthesis, M. Müller for taking the SEM images, K. Kirchoff for taking the TEM images, G.K. Auernhammer, and A. Fery for useful discussion, and B. Ullrich for carefully reading the manuscript. D.V. acknowledges support by the German Science Foundation via SFB TR6 and M.d'A via SPP 1273. A.v.B. acknowledges the Stichting voor Fundamenteel Onderzoek der Materie (FOM), which is supported by the Nederlandse Organisatie voor Wetenschappelijk Onderzoek (NWO).

## References

- 1 E. Mathiowitz, J. S. Jacob, Y. S. Jong, G. P. Carino, D. E. Chickering, P. Chaturvedi, C. A. Santos, K. Vijayaraghavan, S. Montgomery, M. Bassett and C. Morrell, *Nature*, 1997, **386**, 410.
- 2 E. Donath, G. B. Sukhorukov, F. Caruso, S. A. Davis and H. Mohwald, *Angew. Chem., Int. Ed.*, 1998, **37**, 2202.
- 3 S. M. Marinakos, J. P. Novak, L. C. Brousseau, A. B. House, E. M. Edeki, J. C. Feldhaus and D. L. Feldheim, *J. Am. Chem. Soc.*, 1999, **121**, 8518.
- 4 S. M. Marinakos, M. F. Anderson, J. A. Ryan, L. D. Martin and D. L. Feldheim, *J. Phys. Chem. B*, 2001, **105**, 8872.
- 5 P. Tartaj, M. D. Morales, S. Veintemillas-Verdaguer, T. Gonzalez-Carreno and C. J. Serna, *J. Phys. D: Appl. Phys.*, 2003, **36**, R182.
- 6 S. W. Kim, M. Kim, W. Y. Lee and T. Hyeon, *J. Am. Chem. Soc.*, 2002, **124**, 7642.
- 7 S. J. Oldenburg, R. D. Averitt, S. L. Westcott and N. J. Halas, *Chem. Phys. Lett.*, 1998, **288**, 243.
- 8 J. K. Cochran, *Curr. Opin. Solid State Mater. Sci.*, 1998, **3**, 474.
- 9 M. Ohmori and E. Matijevic, *J. Colloid Interface Sci.*, 1992, **150**, 594.
- 10 J. L. West and N. J. Halas, *Curr. Opin. Biotechnol.*, 2000, **11**, 215.
- 11 S. H. Im, U. Y. Jeong and Y. N. Xia, *Nat. Mater.*, 2005, **4**, 671.
- 12 Y. Lu, J. McLellan and Y. N. Xia, *Langmuir*, 2004, **20**, 3464.
- 13 Y. Yin, Y. Lu, B. Gates and Y. Xia, *Chem. Mater.*, 2001, **13**, 1146.
- 14 Y. S. Han, G. Hadiko, M. Fuji and M. Takahashi, *Chem. Lett.*, 2005, 152.
- 15 C. Gao, E. Donath, S. Moya, V. Dudnik and H. Mohwald, *Eur. Phys. J. E: Soft Matter Biol. Phys.*, 2001, **5**, 21.
- 16 O. I. Vinogradova, D. Andrienko, V. V. Lulevich, S. Nordschild and G. B. Sukhorukov, *Macromolecules*, 2004, **37**, 1113.
- 17 V. V. Lulevich, D. Andrienko and O. I. Vinogradova, *J. Chem. Phys.*, 2004, **120**, 3822.
- 18 V. V. Lulevich, S. Nordschild and O. I. Vinogradova, *Macromolecules*, 2004, **37**, 7736.
- 19 V. V. Lulevich and O. I. Vinogradova, *Langmuir*, 2004, **20**, 2874.
- 20 J. Heuvingh, M. Zappa and A. Fery, *Langmuir*, 2005, **21**, 3165.
- 21 F. Dubreuil, N. Elsner and A. Fery, *Eur. Phys. J. E: Soft Matter Biol. Phys.*, 2003, **12**, 215.
- 22 G. B. Sukhorukov, D. G. Shchukin, W. F. Dong, H. Mohwald, V. V. Lulevich and O. I. Vinogradova, *Macromol. Chem. Phys.*, 2004, **205**, 530.
- 23 O. V. Lebedeva, B. S. Kim and O. I. Vinogradova, *Langmuir*, 2004, **20**, 10685.
- 24 O. I. Vinogradova, *J. Phys.: Condens. Matter*, 2004, **16**, R1105.
- 25 M. Carin, D. Barthes-Biesel, F. Edwards-Levy, C. Postel and D. C. Andrei, *Biotechnol. Bioeng.*, 2003, **82**, 207.
- 26 A. E. Smith, Z. B. Zhang, C. R. Thomas, K. E. Moxham and A. P. J. Middelberg, *Proc. Natl. Acad. Sci. U. S. A.*, 2000, **97**, 9871.
- 27 S. G. Shroff, D. R. Saner and R. Lal, *Am. J. Physiol.: Cell Physiol.*, 1995, **269**, C286.
- 28 M. Radmacher, *IEEE Eng. Med. Biol. Mag.*, 1997, **16**, 47.
- 29 C. I. Zoldesi, I. L. Ivanovska, C. Quilliet, G. J. L. Wuite and A. Imhof, *Phys. Rev. E: Stat. Nonlinear Soft Matter Phys.*, 2008, **78**, 051401.
- 30 L. Zhang, M. D'Acunzi, M. Kappl, G. K. Auernhammer, D. Vollmer, C. M. van Kats and A. van Blaaderen, *Langmuir*, 2009, **25**, 2711.
- 31 W. Stöber, A. Fink and E. Bohn, *J. Colloid Interface Sci.*, 1968, **26**, 62.
- 32 H. C. Marsmann, W. Raml and E. Hengge, *Z. Naturforsch., B: J. Chem. Sci.*, 1980, **35**, 1541.
- 33 G. Engelhardt and D. Michel, *High-resolution solid-state NMR of silicates and zeolites*, Wiley, Chichester, 1987.
- 34 A. van Blaaderen and A. P. M. Kentgens, *J. Non-Cryst. Solids*, 1992, **149**, 161.
- 35 J. L. Hutter and J. Bechhoefer, *Rev. Sci. Instrum.*, 1993, **64**, 3342.
- 36 H. J. Butt and M. Jaschke, *Nanotechnology*, 1995, **6**, 1.
- 37 There was a misprint of this equation in the previous paper, Zhang *et al.*, *Langmuir*, 2009.
- 38 L. D. Landau and E. M. Lifshitz, *Elastizitätstheorie*, Akademie Verlag, Berlin, 1991, vol. 7.
- 39 In our previous manuscript we assumed that the PS-film prevented a deformation of the lower hemisphere, Zhang *et al.*, *Langmuir*, 2009.
- 40 A. Fery and R. Weinkamer, *Polymer*, 2007, **48**, 7221.
- 41 W. Koiter, *A Spherical Shell under Point Loads at Its Poles*, Macmillan, New York, 1963.
- 42 E. Reissner, *J. Math. Phys. (Melville, NY, U. S.)*, 1946, **25**, 279.
- 43 T. Adachi and S. Sakka, *J. Mater. Sci.*, 1990, **25**, 4732.
- 44 A. Matsuda, Y. Matsuno, M. Tatsumisago and T. Minami, *J. Sol-Gel Sci. Technol.*, 2001, **20**, 129.
- 45 H. Miguez, F. Meseguer, C. Lopez, A. Blanco, J. S. Moya, J. Requena, A. Mifsud and V. Fornes, *Adv. Mater.*, 1998, **10**, 480.